Direct Electron-to-Carbon Polarization Transfer in Homogeneously Doped Polycarbonates

Mobae Afeworki,† Shimon Vega,‡ and Jacob Schaefer*

Department of Chemistry, Washington University, St. Louis, Missouri 63130

Received November 13, 1991

ABSTRACT: A direct electron-to-carbon DNP solid-effect polarization transfer is observed for the aromatic and carbonyl carbons of polycarbonate homogeneously doped with BDPA (see previous papers for notation). The direct electron-to-carbon polarization transfer operates over a range of 30–60 Å. Carbons that are closest to the free radicals are polarized first and have the longest spin–lattice relaxation times. Fourier transforms of time-domain magnetization, synchronously detected under combined chemical-shift and C–H dipolar interactions, show an asymmetrical sideband pattern in the dipolar frequency dimension. Simulations that *qualitatively* agree with the observed asymmetrical sideband patterns are obtained by assuming that molecular motion in the vicinity of the bulky free radical is reduced.

Introduction

Attempts to transfer polarization from electrons in doped PS across an interface directly to carbons in undoped PC in thin-film PC/PS blends failed (part 1). In this paper, we discuss successful direct *electron-to-carbon* DNP polarization transfers in homogeneously doped polycarbonates. To monitor the DNP-generated carbon magnetization, synchronous sampling was performed as the carbon magnetization evolved under chemical-shift interactions only and under combined chemical-shift and C–H dipolar interactions. In the latter situation, the H–H interactions were suppressed by multiple-pulse decoupling. This synchronous sampling scheme has an advantage over the DRSE technique of part 3 by eliminating the two-rotor-period delay during which electron flips can dephase carbon magnetization. Results obtained from direct electron-to-carbon polarization transfers can be related to electron–carbon distances in the glassy solid state.

Experiments

DNPFT. The DNPFT pulse sequence is an alternate-block, equal-heat, add–subtract pulse sequence with all relaxation delays exactly balanced in the two halves of the experiment. (For a similar sequence, see Figure 5 in part 1.) The first half of the experiment starts with a variable period of microwave irradiation at the difference of the *electron and carbon* Larmor frequencies followed by a 90° inspection pulse on the carbon channel. In the second half of the experiment, the microwave irradiation is delayed until after data acquisition. In both halves, the ^{13}C signal detection begins immediately after the ^{13}C 90° inspection pulse. Protons are decoupled throughout the experiment except during the microwave-irradiation periods. The ^{13}C 90° inspection pulse is cycled through all four phases. A 180° ^{13}C inversion followed by a recovery delay can be placed before the inspection pulse to measure spin–lattice relaxation times of DNP-enhanced carbon signals.

DNPFT Echo. This experiment is similar to the DNPFT experiment just described except the ^{13}C signal is detected as an echo two rotor periods after the ^{13}C inspection pulse. A 180° pulse at the end of the first rotor period refocuses chemical shifts. Microwave irradiation is applied before the ^{13}C inspection pulse in the first half of the experiment, and after data acquisition in the second half. Protons are decoupled except during the microwave-irradiation periods.

Synchronous Detection. Data sampling in the DNPFT and DNPFT-echo experiments was sometimes synchronized with the rotor period. For a spinning speed of 1859 Hz, 16 one-point detections separated by 33.6 μs exactly fit into one rotor period. The synchronous detection is performed in one of two ways (Figure 1). Carbon evolution is observed either under chemical-shift interactions only (C–H dipolar interactions decoupled) or under combined chemical-shift and C–H dipolar interactions (with H–H interactions decoupled by semiwindowless MREV-8 multiple-pulse decoupling). The cycle times of the MREV-8 sequence and the one-point detections are matched, with rotational echo maxima every 16th data point. A variation in the synchronous-sampling experiment involved delaying the H–H multiple-pulse decoupling before the start of the synchronous data acquisition by an integral number of rotor periods during which the C–H interactions are decoupled (Figure 2).

The first few data points in the synchronous-sampling experiment were collected before complete recovery of the spectrometer from the ^{13}C inspection pulse. If the time-domain data were to be analyzed directly without Fourier transforms, the first five points only were left shifted and the data analysis was done by comparing the formation and decay of the first few echoes. Sometimes a 16-point left shift was performed; the data analysis therefore started at the top of the first echo. The 16-point left shift was followed by zero filling to 1-K data points and Fourier transformation with a 20-Hz line broadening. The resulting spectra are referred to as complete Fourier transforms. In some cases, as for instance in using the delayed H–H multiple-pulse decoupling of Figure 2, the data analysis was done by a Fourier transform of the second or third set of 16 time-domain points only, to obtain a 16-point absorption-mode frequency spectrum.

Simulations. Theoretical results were obtained by numerical calculations using a computer program[1] constructed to simulate NMR signals under a variety of interactions and magic-angle spinning speeds on a two-spin system (both spin $^1/_2$). The interactions included chemical shift *only*, and chemical shift *plus* C–H dipolar, with no H–H interactions. The calculations were modified to include two-site jumps that simulated the π flips of the phenyl rings of polycarbonate.

Results

DNPFT. The ^{13}C DNP difference signals for PC(*) (Figure 3, top left) and PC(^{13}C/*) (Figure 4, top left) indicate direct electron-to-carbon polarization transfer. All of the ^{13}C center bands of PC(*) show DNP enhancements but to varying degrees. The carbonyl-carbon peak is enhanced the most. The enhancement of the methyl-carbon peak at 30 ppm is negative. This enhancement was positive when the protons were irradiated by a string of 90° pulses during the microwave irradiation period (data not shown). The DNP difference spectrum of PC(^{13}C/*) obtained with 0.5-s microwave irradiation has relatively more of a broad component than the spectrum

† Present address: Exxon Research and Engineering Co., Annandale, NJ 08801.

‡ Permanent address: Department of Chemical Physics, The Weizmann Institute of Science, Rehovot 76100, Israel.

0024-9297/92/2225-4100$03.00/0

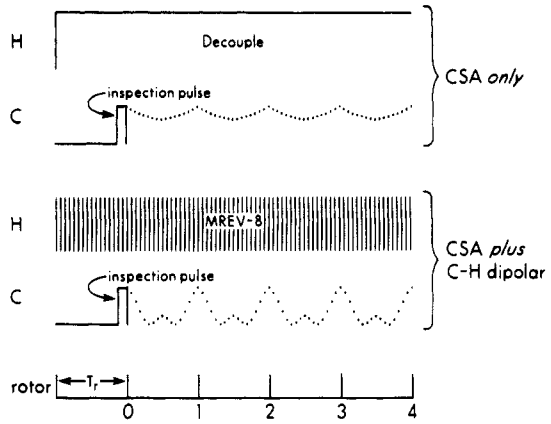

Figure 1. Pulse sequences for synchronous sampling data acquisition. A 5.0-μs 90° inspection pulse on the carbon channel is followed by data acquisition every 33.6 μs with either full C–H decoupling at 87 kHz (top) or multiple-pulse H–H decoupling (bottom). The one-point detections, represented by dots in the figure, are synchronized with both the cycle time of the semiwindowless MREV-8 sequence (t_c = 33.6 μs) and the rotor period (16 × 33.6 μs = 538 μs). The ^{13}C inspection pulse is preceded by a one rotor-period preparation period.

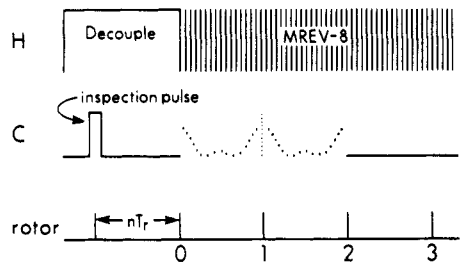

Figure 2. Pulse sequence for delayed MREV-8 decoupling and synchronous detection. The experiment begins with a ^{13}C inspection pulse followed by C–H decoupling for an integral number of rotor periods. The magnetization is then allowed to evolve under combined chemical-shift and C–H dipolar interactions. Synchronous sampling (solid circles) is performed with H–H interactions suppressed by semiwindowless MREV-8 multiple-pulse decoupling. The nT_r delay selects carbons that are distant from the free-radical centers.

obtained with 2.0-s microwave irradiation (Figure 5, left). On the basis of the results of an inversion recovery experiment (Figure 5, right), the broad component has a relatively long T_1(C).

DNPFT Echo. The results of DNPFT-echo experiments performed on PC(*) and PC(^{13}C/*) also show direct electron-to-carbon polarization transfer (Figures 3 and 4, right). The vertical scaling of all six spectra of Figure 4 is the same, allowing direct comparisons between the DNPFT and DNPFT-echo results on PC(^{13}C/*). The DNPFT-echo spectra have narrower lines relative to those obtained by DNPFT. The methyl-carbon peak of PC(*) shows a negative DNP enhancement in the echo spectra, which, because of the absence of broad resonances, is more obvious in the echo spectra than in the normal spectra. Contributions to the broad component are almost completely dephased by the end of the second rotor period. After 1 s of microwave irradiation, the DNP enhancements of resonances of the carbonyl carbon, protonated aromatic carbons, nonprotonated aliphatic carbons, and methyl carbons are 7, 2, 3, and −1, respectively (Figure 3, right, bottom, and middle).

Synchronous Sampling. The first four synchronously sampled echoes for PC(^{13}C) and PC(^{13}C/*) are displayed as phase-independent relative magnitudes in Figure 6. The rotational-echo maxima for PC(^{13}C) under the chemical-shift interaction only decay with a time constant of 4.0 ms

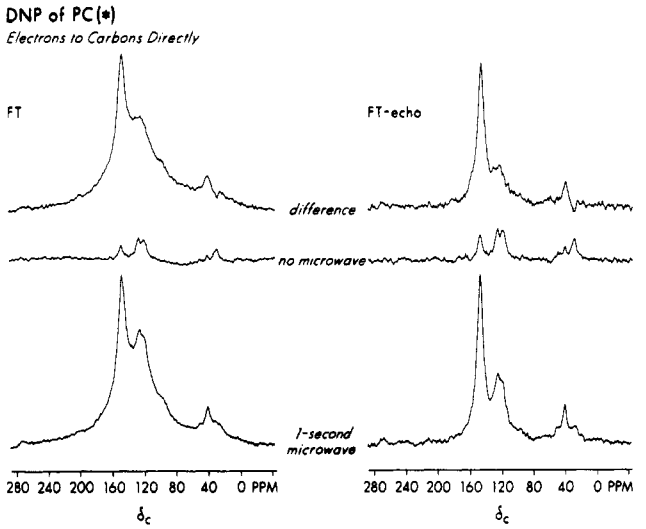

Figure 3. 15.1-MHz DNPFT and DNPFT-echo ^{13}C NMR spectra of PC(*) following direct electron-to-carbon polarization transfer. The spectra on the left are the result of a DNPFT experiment with (bottom) and without (middle) 1-s microwave irradiation. The spectra on the right are the result of a DNPFT-echo experiment with (bottom) and without (middle) 1-s microwave irradiation. The top spectra are differences (bottom minus middle). In both sets of spectra the methyl-carbon peak at 30 ppm shows a negative DNP enhancement due to an electron–proton–carbon *three-spin effect*.

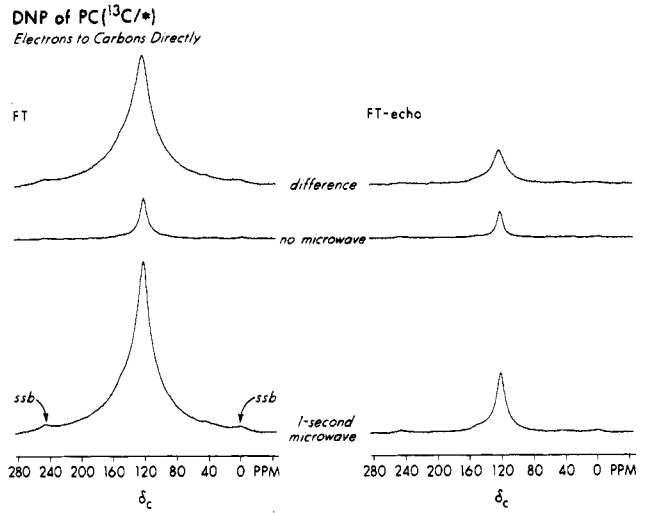

Figure 4. 15.1-MHz DNPFT and DNPFT-echo ^{13}C NMR spectra of PC(^{13}C/*) following direct electron-to-carbon polarization transfer. The spectra on the left are the result of a DNPFT experiment with (bottom) and without (middle) 1-s microwave irradiation. The spectra on the right are the result of a DNPFT-echo experiment with (bottom) and without (middle) 1-s microwave irradiation. The top spectra are differences (bottom minus middle). In both cases a total of 2064 scans were averaged. The vertical display scale for all six spectra is the same.

(Figure 6, top). The evolution of the magnetization for PC(^{13}C/*) under combined chemical-shift and C–H dipolar interactions is dephased within each rotor period and refocused at the end of a rotor period (Figure 6, middle). The resulting rotational-echo maxima decay with a time constant of 1.3 ms. The decay of the echo maxima of the direct electron-to-carbon, DNP-enhanced magnetization for PC(^{13}C/*) under combined chemical-shift and C–H dipolar interactions has a time constant of 1.0 ms. The time constant of the decay of the echo train for PC(^{13}C/*) for chemical-shift interactions only was 2.1 ms (data not shown). The displays of the refocusing and dephasing of the first echo for PC(^{13}C) and PC(^{13}C/*) under combined

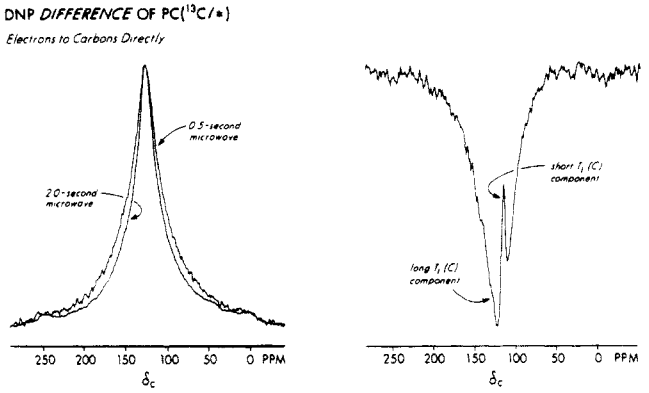

Figure 5. (Left) DNPFT ^{13}C NMR *difference* spectra of PC-($^{13}C/*$) with 0.5- and 2.0-s microwave irradiation at the difference of the electron and *carbon* Larmor frequencies. The experiments were done as an alternate-block, add–subtract, equal-heat acquisition with all relaxation delays balanced. The difference spectra were generated by averaging 2000 scans in each of the two blocks. (Right) DNPFT ^{13}C NMR difference spectrum with 2-s microwave irradiation 800 ms after a 180° ^{13}C inversion pulse.

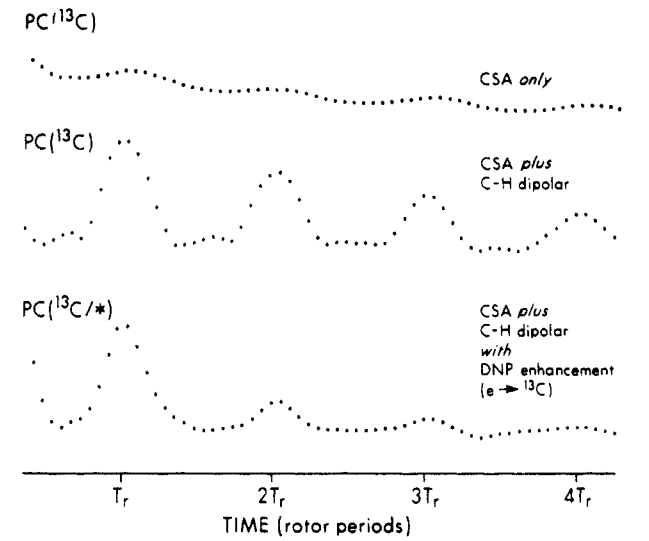

Figure 6. Magnitudes of PC rotational echoes acquired synchronously using the pulse sequences shown in Figure 1. The evolution of the carbon magnetization was measured under chemical-shift interactions only (top) and under combined chemical-shift and C–H dipolar interactions with H–H interactions decoupled by semiwindowless MREV-8 multiple-pulse decoupling (middle and bottom) for PC(^{13}C) (top and middle) and PC($^{13}C/*$) (bottom). Only 64 of 256 data points acquired are shown with the first five data points removed. Most of the signal has disappeared by $2T_r$ for the BDPA-doped PC.

chemical-shift and C–H dipolar interactions are expanded in Figure 7.

The Fourier transforms of the time-domain data of Figure 6 are asymmetrical about the center band. Negative spinning sidebands appear at $n = -2$ and -3 for PC(^{13}C) (Figure 8, top) but not for PC($^{13}C/*$) (Figure 9, top). All of the peaks in the PC($^{13}C/*$) dipolar spectrum have DNP enhancements, with the natural-abundance ^{13}C nonprotonated, aromatic-carbon peak enhanced the most (arrow, Figure 9, bottom). The enhanced peaks are superimposed on a broad resonance that appears to be shifted by about 1 kHz to low field (Figure 9, bottom).

The asymmetry of the dipolar sideband pattern for PC-(^{13}C) differs from that for PC($^{13}C/*$) (Figure 8) even though both samples have the same chemical-shift anisotropy. The latter was confirmed by the ratio of the intensities of the first spinning sidebands to their respective center bands (MAS = 1859 Hz) in an experiment in which the evolution of the magnetization was under chemical-shift interactions only (data not shown).

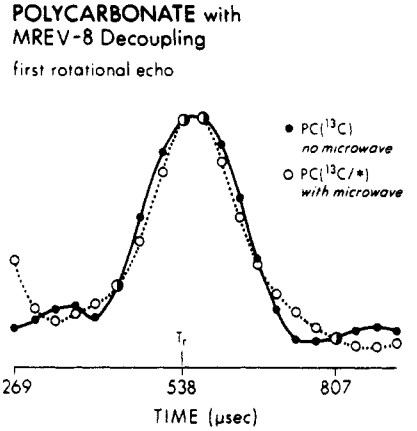

Figure 7. First echo for PC(^{13}C) and PC($^{13}C/*$) with evolution under combined chemical-shift and C–H dipolar interactions. The formation and dephasing for the free-radical doped sample are faster than those for the undoped sample. Data points are connected by solid and dotted lines to guide the eye.

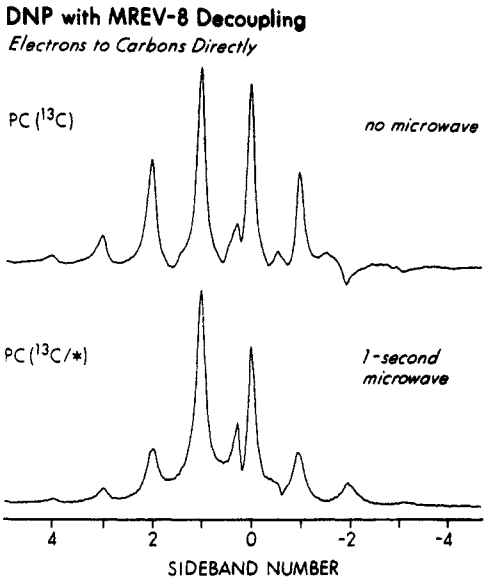

Figure 8. Fourier transforms of the time-domain data shown in Figure 6 (middle and bottom) with $t = 0$ defined by the top of the first echo.

Simulations. Simulated spectra corresponding to evolution of carbon magnetization chemical-shift interactions only and of C–H dipolar interactions only were adjusted to match the experimental results (Figure 10). The dipolar coupling and the principal components for the chemical-shift tensor used in fitting the simulated spectra to the experimental spectra are presented in Table I. The parameters obtained from these fits were used to predict spectra obtained under CSA interactions only, and under combined CSA and C–H dipolar interactions for 1859-Hz magic-angle spinning (Figure 11, bottom). The asymmetry of the latter spectrum is pronounced even though the chemical-shift interaction is weak and the dipolar interaction symmetric.

Simulations that incorporate chemical-shift and C–H dipolar interactions assuming the applicability of a two-site jump model for the protonated, aromatic carbon match experimental 16-point stick spectra resulting from the Fourier transforms of synchronously sampled carbon-magnetization evolution (Figure 12). For these transforms, $t = 0$ was defined by the top of the first echo after delayed H–H decoupling (see Figure 2). The matches were best for two and three rotor-period delays with H–C decoupling.

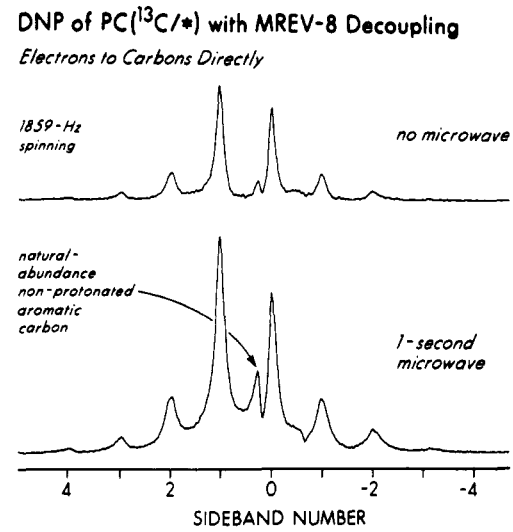

Figure 9. Fourier transforms of the time-domain data of the synchronous-acquisition experiments of Figure 1 on PC(^{13}C/*) with (bottom) and without (top) 1-s microwave irradiation. The microwave irradiation was followed by a one rotor-period preparation with MREV-8 decoupling prior to the ^{13}C inspection pulse. The Fourier transform was performed with $t = 0$ defined by the top of the first echo by left shifting the first 16 points, zero filling to 1-K data points, and applying a 20-Hz line broadening. The natural-abundance ^{13}C nonprotonated, aromatic-carbon line is strongly enhanced (arrow). This spectrum also appears at the bottom of Figure 8. A total of 37 000 scans were collected to generate each spectrum.

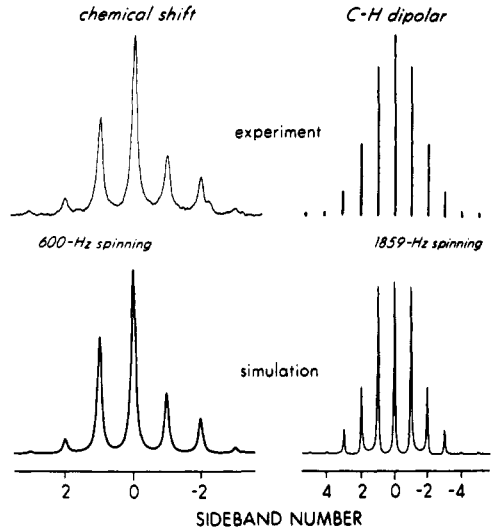

Figure 10. Experimental and simulated spectra of the protonated, aromatic-carbon magnetization at 15.1 MHz of PC under chemical-shift interactions *only* (left) and under C–H dipolar interactions *only* (right). The calculated fit to the dipolar spectrum is only approximate because the effects of nonflip motions were not included. The parameters used in the simulations are given in Table I.

Discussion

Direct Electron-to-Carbon Polarization Transfer. The ^{13}C difference signals observed for PC(*) and PC(^{13}C/*) using the DNPFT and DNPFT-echo sequences (Figures 3 and 4) are proof of a direct electron-to-carbon polarization transfer. The ^{13}C resonances observed in the DNPFT experiments are broader than those observed in the DNPFT-echo experiments (1500 Hz compared to 200 Hz). Carbons that are closer to the paramagnetic centers are the first to be dephased by electron flips. These are also the carbons that are polarized first (Figure 5, left) and the carbons with the longest T_1(C) (Figure 5, right), the latter presumably the result of a combination of restrictions on motion imposed by the bulky free radical (part 3) and the selectivity of the DNP enhancement process for sites with little spin–lattice leakage (part 1). We estimate that an electron–carbon dipolar broadening of 1500 Hz corresponds to a distance of 30 Å, and a broadening of 200 Hz corresponds to a distance of about 60 Å.

Table I
Parameters for Simulations

	σ_{xx} (kHz)	σ_{yy} (kHz)	σ_{zz} (kHz)	D_{CH} (kHz)	MAS (kHz)	flip angle (deg)
CSA only	0.300	1.100	−1.400		0.600	
CSA only	0.300	1.100	−1.400		1.859	
CSA plus C–H dipolar	0.300	1.100	−1.400	9.0	1.859	
C–H dipolar only				9.0	1.859	
CSA plus C–H dipolar with two-site jumps	0.300	1.100	−1.400	9.0	1.859	180

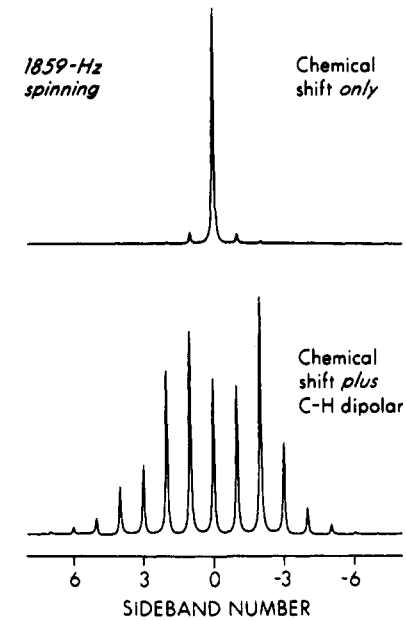

Figure 11. Simulations of sideband patterns for protonated, aromatic-carbon magnetization at 15.1 MHz of PC under chemical-shift interactions *only* (top) and combined chemical-shift *plus* C–H dipolar interactions under magic-angle spinning at 1859 Hz. The asymmetries in the patterns arise from the anisotropic chemical shift.

The DNP enhancement for the PC protonated, aromatic carbon under a direct electron-to-carbon transfer is about 4 (Figure 3, left). This is the same enhancement observed for the protons of PC and only one-fourth of the expected enhancement. The fast transfers to carbons occur over 30 Å, which was probably not quite sufficient to span the irregular interface separating electrons and PC carbons in the thin-flim PC/PS blends described in part 1. Slower transfers to more distant carbons which have narrower, more easily detected lines, must still compete with the leakage due to fast ^{13}C spin–lattice relaxation. The combination of low sensitivity and broad lines explains the failure to detect an interface-PC echo signal after two rotor periods by direct electron-to-carbon transfer as reported in parts 1 and 2.

Three-Spin Effect. The chemically different carbons of PC(*) have varying DNP enhancements (Figure 3) reflecting differences in their T_1's and DNP leakage factors. The enhancement of the carbonyl-carbon peak at 150 ppm is about 3 times that of the other carbons, consistent with the carbonyl-carbon T_1 of 10 s,[2] compared to T_1's of about 0.2 and 0.1 s for the methyl carbons and the protonated, aromatic carbons, respectively.[3]

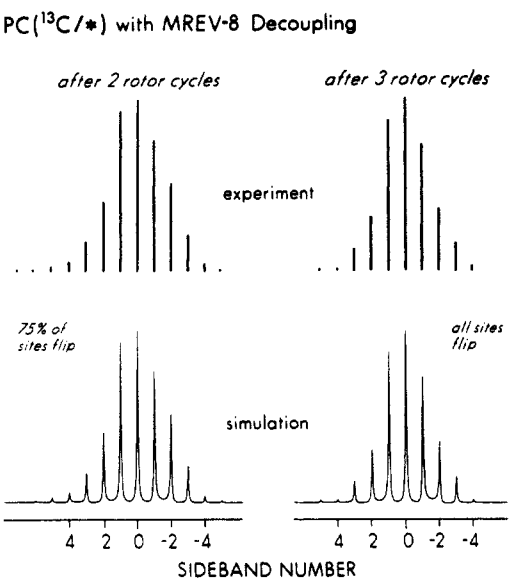

Figure 12. Experimental and simulated spectra of the protonated, aromatic-carbon magnetization of PC(^{13}C/*). The experimental spectra are the results of a delayed-decoupling experiment (Figure 2) after two (top left) and three (top right) rotor periods of C–H decoupling following the inspection pulse. The bottom two spectra are simulations with chemical-shift and C–H dipolar interactions assuming a two-site jump model for ring flips in which only 75% of the rings flip (bottom left) and all rings flip (bottom right).

The negative DNP enhancement of the methyl carbons is due to a *three-spin effect*, first observed in solution DNP NMR studies of electron–proton–carbon coupling[4] and electron–proton–fluorine coupling,[5,6] and more recently in solid DNP NMR studies of electron–proton–carbon coupling.[7] The three-spin effect is observed in cases where one of two nuclei is more strongly polarized by the electron than the other, and the two kinds of nuclear spins are strongly coupled to each other. Theoretical descriptions of the three-spin effect may be found in refs 4 and 8. The microwave irradiation at the difference of the electron and carbon Larmor frequencies is sufficiently close to resonance for the electrons that protons can be polarized by an Overhauser DNP effect, assuming the presence of fast molecular motion of the protons relative to the electrons. Only the methyl-carbon resonance has a negative DNP enhancement because the short correlation time of the internal methyl-carbon C_3 rotation indicates fast motion of the protons. When the protons of PC(*) were saturated by a string of uniformly-spaced proton 90° pulses during the microwave-irradiation period, all of the ^{13}C DNP enhancements were positive, proving that the negative DNP enhancement is indeed due to a three-spin Overhauser effect. Similar results have been reported by Maresch et al.[9] on other polymer systems.

Synchronous Sampling and Asymmetrical Sideband Patterns. The spinning sidebands observed for PC(^{13}C) and PC(^{13}C/*) in the synchronous-sampling experiments under chemical-shift interactions only (C–H dipolar interactions decoupled) are small compared to the center bands because of the small chemical shift anisotropies at the relatively low field of 1.4 T. The ratio of the intensities of the first sidebands to the center band is 4% or less in both PC(^{13}C) and PC(^{13}C/*) spectra. In H–H multiple-pulse decoupled synchronous sampling, an asymmetrical pattern is expected because the effect on evolution of the chemical-shift tensor is included. The synchronous-detection experiments were performed with no chemical-shift selectivity. Each time-domain data point represents all carbons regardless of their chemical-shift tensor or offset. Although the major contributor to the spectra of Figures 8 (bottom) and 9 is the ^{13}C-enriched, protonated, aromatic carbon, all other carbons make contributions.

The simulated spectrum obtained under the combined CSA and C–H dipolar interactions *qualitatively* agrees with the spectrum obtained experimentally in that the experimental and simulated spectra are asymmetric about the center band. But the details do not match: for example, both $n = 2$ and $n = -2$ sidebands of the simulated spectrum are more intense than the center band (Figure 11, bottom), while the experiment shows an intense $n = 2$ sideband, but a negative-going $n = -2$ sideband, for PC(^{13}C) (Figure 8, top). Negative sidebands can result from incomplete powder averaging, but in our case the evolution occurred over complete rotor periods and negative sidebands are not expected. We believe that the negative sidebands could be due to intermolecular ^{13}C–^{13}C interactions that do not refocus at the rotor period. In addition, contributions from nonprotonated aromatic carbons are possible. The nonprotonated, aromatic-carbon peaks are frequency offset with respect to the protonated, ^{13}C-labeled, aromatic-carbon resonances. The offsets could accumulate phase to create the appearance of negative sidebands. The shifted broad line (Figure 8, bottom) may indicate an isotropic shift arising from specific orientations of PC chains closest to BDPA.

The delayed H–H decoupling sequence of Figure 2 selects carbons distant from the free-radical centers. Most of the carbons that are close to BDPA are dephased by the end of the second rotor period, as shown by the weak echo intensity of the broad component in Figure 4. Stick spectra obtained by Fourier transforms of 16 time-domain points from delayed data acquisition match simulations that incorporate chemical-shift and C–H dipolar interactions *and* two-site jumps of the phenyl rings (Figure 12). The spectra were obtained from the time-domain data collected after two and three rotor-period delays in the MREV-8 multiple-pulse decoupling. A simulated spectrum with 75% of the sites undergoing two-site ring flips matches the stick spectrum after a two rotor-period delay in the H–H multiple-pulse decoupling. The simulated spectrum with all sites undergoing two-site jumps (as in bulk PC) matches the experimental spectrum after a delay of three rotor periods in the MREV-8 decoupling. This suggests that motion only in the vicinity of the free radical is reduced. The match between experiment and simulation should be considered *qualitative* because intermediate-frequency motions that affect the line shape are not represented in the simulations. Nevertheless, we conclude that a narrow carbon resonance is a guarantee of sufficient distance from BDPA that molecular dynamics are not affected. Thus the conclusions about PC dynamics at interfaces reported in part 3 are free from complications due to distant BDPA in PS.

Time-Domain Analysis. The time-domain data shows that the BDPA-doped PC has echoes that both form and are dephased faster than echoes in PC (Figure 7). Doped PC therefore has a broader distribution of sidebands in the dipolar frequency domain. A broader distribution of sidebands in the dipolar domain means that BDPA-doped PC has more restricted motion, that is, PC chains are less mobile in the presence of BDPA. This is the same conclusion reached on the basis of analysis of the frequency-domain data of Figure 12. Presumably, the bulk of BDPA affects chain packing and disrupts coordinated PC chain motion. In other words, BDPA acts as an antiplasticizer.[10] We believe that the broadening of the distribution of sidebands is not the result of electron flips,

which are on a millisecond time scale, interferring with the efficiency of the MREV-8 decoupling because of the symmetry of the PC(^{13}C/*) echo near its center (Figure 7).

Conclusion

In these four papers we have demonstrated the practicality of using 50-Å, direct electron-nuclear polarization transfers for both selectivity and sensitivity in characterizing the interfaces of immiscible, amorphous polymers by NMR spectroscopy. The double thin-film technique for doping one component of an immiscible blend with a noncovalently bound stable free radical is general, so long as a solvent–nonsolvent pair can be found for the two polymers of the blend. When chemical-shift differences between doped and undoped polymers are not large, stable-isotope labeling can be used to distinguish components. Once the polarization transfer has been made, standard NMR relaxation experiments measure the microscopic motions of those chains in the undoped phase which are at the interface, with no interferences from the free radical. The results obtained so far for a model of the commercially important blend of polycarbonate and polystyrene indicate that polycarbonate chains near the interface are immobilized, probably the result of local, atypical variations in packing density. It remains for future studies to examine this packing as a function of thermal history and exposure to solvents and compatibilizers to connect the mechanical properties of the blend with structure and dynamics of chains at the interface.

Acknowledgment. This work has been supported by the Office of Naval Research.

References and Notes

(1) Olejniczak, E. T.; Vega, S.; Griffin, R. G. *J. Chem. Phys.* **1984**, *81*, 4804.
(2) Henrichs, P. M.; Linder, M.; Hewitt, J. M.; Massa, D.; Isaacson, H. V. *Macromolecules* **1984**, *17*, 2412.
(3) Walton, J. H.; Lizak, M. J.; Conradi, M. S.; Gullion, T.; Schaefer, J. *Macromolecules* **1990**, *23*, 416.
(4) Hausser, K. H.; Reinbold, F. *Phys. Lett.* **1962**, *2*, 53.
(5) Richards, R. E.; White, J. W. *Proc. Chem. Soc.* **1962**, 119.
(6) Richards, R. E.; White, J. W. *Discuss. Faraday Soc.* **1962**, *34*, 96.
(7) Duijvestijn, M. J.; Wind, R. A.; Smidt, J. *Physica* **1986**, *138B*, 147 and references therein.
(8) Natusch, D. F. S.; Richards, R. E.; Taylor, D. *Mol. Phys.* **1966**, *11*, 421.
(9) Maresch, G. G.; Kendrick, R. D.; Yannoni, C. S.; Galvin, M. E. *J. Magn. Reson.* **1989**, *82*, 41.
(10) Wehrle, M.; Hellmann, G. P.; Spiess, H. W. *Colloid. Polym. Sci.* **1987**, *265*, 815.